

Article

# Hurricane Ian Damage Assessment Using Aerial Imagery and LiDAR: A Case Study of Estero Island, Florida

Leanne Hauptman <sup>1</sup>, Diana Mitsova <sup>2,\*</sup> and Tiffany Roberts Briggs <sup>1</sup>

<sup>1</sup> Department of Geosciences, Florida Atlantic University, Boca Raton, FL 33431, USA; lhauptman2021@fau.edu (L.H.); briggst@fau.edu (T.R.B.)

<sup>2</sup> Department of Urban and Regional Planning, Florida Atlantic University, Boca Raton, FL 33431, USA

\* Correspondence: dmitsova@fau.edu

**Abstract:** Remote sensing techniques have emerged as an essential tool for conducting damage assessments and are commonly used to improve disaster recovery planning and community resilience policies. The objective of this study was to use aerial imagery data and LiDAR to identify the hardest hit areas, quantify the extent of damages, and compare pre- and post-storm beach morphology conditions in Estero Island, Florida, relating to Hurricane Ian in 2022. This study identified >2400 structures that were impacted by Hurricane Ian, with 170 structures suffering extensive damage. Clustering of heavily damaged buildings was observed on the northern and central portions of the island, with lower levels of damage clustered on the southern part. Among the ‘severely damaged’ and ‘destroyed’ structures were seven mobile home subdivisions. The total assessed value of the heavily damaged structures was estimated at over USD 200 million. The results also indicated substantial post-storm debris and sand deposition across the entire island. Remote sensing provides advanced techniques that can help prioritize emergency response efforts after catastrophic impacts from a natural disaster.

**Keywords:** beach morphology; hurricane; emergency response; supervised classification; remote sensing; LiDAR; JABLTCX



**Citation:** Hauptman, L.; Mitsova, D.; Briggs, T.R. Hurricane Ian Damage Assessment Using Aerial Imagery and LiDAR: A Case Study of Estero Island, Florida. *J. Mar. Sci. Eng.* **2024**, *12*, 668. <https://doi.org/10.3390/jmse12040668>

Academic Editor:  
Theocharis Plomaritis

Received: 25 February 2024  
Revised: 9 April 2024  
Accepted: 13 April 2024  
Published: 17 April 2024



**Copyright:** © 2024 by the authors. Licensee MDPI, Basel, Switzerland. This article is an open access article distributed under the terms and conditions of the Creative Commons Attribution (CC BY) license (<https://creativecommons.org/licenses/by/4.0/>).

## 1. Introduction

Hurricane Ian made landfall in Lee County, Florida, on 28 September 2022, as a Category 4 storm with wind speeds of 155 mph and up to 4 m of storm surge. Hurricane Ian was among the strongest storms to hit the United States, with the highest recorded storm surge documented in Southwest Florida in the past 150 years [1,2]. Initial damage assessments show Hurricane Ian caused more than USD 112 billion in combined damage to residential and commercial structures [3]. In addition to loss of lives, flooding, and wind damage, the storm caused significant coastal change that eroded coastal habitats, damaged homes and infrastructure, and led to the collapse of several bridges [2]. Studying the immediate impacts of storm events is crucial to assisting governmental agencies in rapid response and recovery operations.

Damage assessments after hurricane strikes have a long history in Florida and other coastal areas. Ball et al. [4] investigated the geologic framework of Hurricane Donna and damages to the reef tract and beach morphology using photographs, cores, maps, and bottom markers in the 1960s. Contemporary damage assessments now focus on rapid assessments and advanced remote sensing technologies in efforts to shorten the feedback loop between assessment, response, and recovery operations. Rapid hurricane damage assessments have traditionally been conducted through field reconnaissance deployments, but these methods can be labor-intensive, costly, and risky for the personnel involved [5]. Remote sensing techniques have emerged as a critical tool for conducting coastal change and damage assessments to improve recovery planning and enact more effective policies and

procedures that can enhance community resilience. Airborne remote sensing technologies such as aerial imagery and airborne LiDAR can be utilized to collect time-critical geospatial data after a disaster [6] and determine post-disaster coastal change and flood damage extents [7]. Several studies have examined different remote sensing techniques to quantify post-disaster damage accurately and incorporate these assessments into future community resilience planning.

Although several studies have investigated the impacts of hurricanes using remote sensing technology [8–11], relatively limited attention has been given to applying a multi-faceted approach that links damage assessment to post-storm changes in barrier island morphology. Bhatt et al. [12] conducted a study of the geomorphological impacts of Hurricane Ian to quantify net sediment loss and gain to southwestern Florida barrier islands using drone-flown LiDAR and NOAA Digital Terrain Models (DTM). The use of an unmanned aircraft to collect LiDAR immediately following Hurricane Ian allowed for a rapid assessment of morphological change in the study area. However, only geomorphology was investigated, without further examination of structural damages or related impacts to the built environment. Robertson et al. [13] investigated the spatial variation in beach morphology pre- and post-Hurricane Ivan in Panama City, Florida, using a unique, high-resolution airborne laser dataset. The study provided quantification of large-scale post-hurricane beach morphological changes.

Other studies have primarily focused on estimating post-hurricane structural damages [7,14–17]. Zhou et al. [15] conducted a detailed residential building damage assessment after Hurricane Sandy using image-based three-dimensional (3D) reconstruction of buildings. More specifically, the study used street-level photography and mobile LiDAR to evaluate the applicability of 3D image reconstruction in post-hurricane assessments. The study revealed that image-based 3D reconstruction can adequately support hurricane damage assessments. Xian et al. [17] conducted a rapid assessment of damaged residential buildings in the Florida Keys after Hurricane Irma in 2017. Using NOAA's post-storm satellite imagery, the investigators identified the hardest hit areas to conduct a rapid field reconnaissance assessment. Over 3700 images obtained from field reconnaissance surveys were coupled with satellite imagery to complete the damage assessment [17]. While these assessments provided extensive details of damage to a single structure, the methodology requires data to be physically gathered by a foot-on-ground approach. Gong and Maher [14] examined the potential of mobile LiDAR for post-disaster geospatial data collection by examining the impacts of Hurricane Sandy through field surveys using a mobile LiDAR method that was propped onto a car. The study demonstrated how the detailed information gathered from land-based mobile LiDAR can improve rapid response and assist local decision making. However, this methodology can be time-consuming and resource-intensive, especially when conducting rapid assessments of disaster impacts. In addition, it has limited applicability if the study area is not easily accessible due to debris or collapsed roads and bridges.

Davis et al. [7] conducted a damage assessment using the ADCIRC (Advanced CIRCulation Model for Coastal Ocean Hydrodynamics) [18] storm surge model, image classification, and LiDAR to produce a rapid damage assessment after Hurricane Michael in the Florida Panhandle. The study classified over 700 buildings based on the scale of damage and estimated the economic value of the affected structures. However, the study only focused on examining elevation and did not consider beach morphological conditions. Battersby et al. [16] proposed an empirical study to identify the coarsest spatial resolution that is adequate for damage assessment immediately following a major disaster. Using a cognitive science approach, the study found that a spatial resolution of 1.5 m and above has limited utility for identifying structural damage. The approach from this study offers a threshold for remote sensing techniques like aerial imagery to be utilized in categorizing the extent of damages after a natural disaster based on visual interpretation and expert judgment.

Hurricanes in the past decade have devastated many coastal communities, disrupting the daily lives of millions (i.e., 2005 Hurricane Katrina, 2012 Hurricane Sandy, 2017 Hurri-

cane Irma, and 2017 Hurricane Harvey, among others). Recent climatic research indicates that hurricanes may intensify, which can increase flood risk and the vulnerability of coastal communities [19]. Continued rapid damage assessments after a disaster are critical for rescue, recovery, and emergency planning. Emergency managers, utility providers, and local decision makers will increasingly rely on methodologies supporting rapid evaluation of disaster impacts, identifying response priorities, and analyzing alternative community recovery strategies. Lack of access to impacted areas after a catastrophic storm often creates significant challenges in accomplishing these goals [15]. Remote sensing offers advanced techniques to gather extensive data after a natural disaster and the ability to analyze large-scale datasets relatively quickly.

Barrier islands worldwide are experiencing both the pressure of urban development and the impacts of more frequent and intense storms. Barrier islands are elongated wave-, tide-, and wind-built ridges that are composed predominantly of unconsolidated sand and gravel [20]. While these low-lying islands provide protection to the adjacent mainland from high water levels caused by storms, barrier islands are susceptible to erosion [20]. As sea levels rise and hurricanes intensify, barrier islands become more vulnerable, as dune systems can be readily overtopped by higher storm surges [21], leaving adjacent communities increasingly exposed to natural disasters.

The objective of this study is to use aerial imagery and airborne LiDAR to examine structural damage and debris deposition relative to barrier island morphological changes resulting from hurricane impacts. More specifically, the study seeks to quantify the extent of damages and compare pre- and post-storm beach morphology conditions for Estero Island, Florida, in the aftermath of Hurricane Ian (23 September 2022–30 September 2022). Although the focus of this study is on a small barrier island in Florida, the approach is generalizable, as it provides a conceptual framework for a more comprehensive disaster impact assessment by integrating three streams of scientific inquiry and analysis: beach morphological change using beach profile analysis, debris and sediment deposition assessment using supervised classification, and structural damage assessment using remote sensing and LiDAR. The results from this study can help improve disaster planning by developing new policies and guidelines for coastal development in some of the most vulnerable and storm-exposed areas [22].

## 2. Methods

### 2.1. Study Area

Lee County includes eight low-lying barrier islands with elevations from 1.8 m to 3.6 m NGVD [23]. Estero Island, which is the focus of this study (Figure 1), was formed by an ample supply of sediment over a relatively low shelf gradient offshore with a north-south orientation [6,24,25]. Estero Island is influenced by a mixed tidal regime with wave heights ranging from 0.01 m to 0.3 m, except during weather events [26,27]. Estero Island has experienced critical erosion and is designated as a critically eroded area by the Florida Department of Environmental Protection (FDEP) [26]. To address this ongoing concern, Lee County's Coastal Advisory Council and the Division of Natural Resources work with government agencies to restore and maintain the beaches. Lee County completed the Estero Island Beach Restoration Project in 2011, placing 403,000 cubic yards along the 6700 feet of the north-central segment of the island. A terminal groin was added on the northern end of the beach fill [28,29]. In 2016, the U.S. Army Corps of Engineers (USACE) dredged Matanzas Pass, adding about 130,000 cubic yards of dredged material to the nearshore on the northern portion of the island [28]. In 2017, Lee County imported approximately 2100 cubic yards of material via truck haul for emergency nourishment after the impacts of Hurricane Irma [28]. The barrier island is subject to extensive development as it is adjacent to Fort Myers, one of the fastest-growing Florida cities [6,30].



**Figure 1.** Extent of study area, Estero Island, Florida, and Hurricane Ian track.

Hurricane Ian was among the most destructive hurricanes to ever hit Florida. On 28 September, Category 4 Hurricane Ian made landfall along the southwestern coast of Florida near Estero Island. Maximum inundation levels of 8 to 12 feet AGL occurred on the island. A USGS water level sensor measured a wave-filtered water level of 12.70 ft above MHHW at Fort Myers Beach Pier [31]. Estero Island experienced some of the worst storm surge events [31]. Hurricane Ian caused sustained beach and dune erosion throughout Estero Island, including major storm surge discharge gullies [32]. Estero Island has a planned renourishment of 905,000 cubic yards of sand placement (expected to begin in 2024). However, the authorities are seeking funds to replace up to 221,000 cubic yards of additional sand lost to Hurricane Ian [32].

## 2.2. Data Processing

The primary datasets used in the analysis included aerial imagery and airborne LiDAR point cloud data. Pre-storm imagery (collected via orthophotography from 1 January to 11 March 2022) was obtained from Lee County's open-source Geographic Information Systems portal. The imagery was color aerial orthophotography provided in MrSid format with a 3-inch ground pixel size. Post-storm imagery was obtained from the National Geodetic Survey Emergency Response Imagery database operated by the National Oceanographic and Atmospheric Administration (NOAA) [33]. The database provides high-resolution aerial imagery of extreme weather events from 2003 to the present. Hurricane Ian imagery was collected by a series of aerial survey missions conducted by a NOAA aircraft from 29 September to 3 October 2022 [33].

Airborne LiDAR for pre- and post-storm was obtained from the Joint Airborne LiDAR Bathymetry Technical Center of Expertise (JALBTCX). The data were collected by the Coastal Zone Mapping and Imaging Lidar (CZMIL) system. JALBTCX is a partnership among the federal government, industry, and academia to perform operations, research, and development in airborne LiDAR bathymetry and complementary technologies [34]. The CZMIL topographic data were compiled to meet a 20 cm vertical accuracy and a 1 m horizontal accuracy at the 95% confidence level. Once the raw LiDAR point cloud data

were obtained from JALBTCX, data processing was completed using LiDAR Analyst™ (<https://www.textronsystems.com/products/lidar-analyst>, accessed on 15 December 2023), an extension to ESRI Geographic Information System (GIS) software. The LAS dataset was processed into a first return Digital Elevation Model (DEM) to visualize the point cloud in 2D and to give a point reference for later processing of BareEarth DEMs and building extractions. Coordinate systems were set to a projected coordinate system of NAD 1983 (2011) State Plane Florida West, and a vertical coordinate system was set to NAVD88 in meters. Using the Extract BareEarth tools in LiDAR Analyst™, a BareEarth DEM was generated based on the first return. The Extract Buildings tool in LiDAR Analyst™ offered a quick and easy extraction of building footprints and associated attributes. Building footprints were extracted from both the pre- and post-storm LiDAR dataset to ensure the quality of the post-storm damage assessment. The Select By Location tool in ArcGIS was used to select all extracted pre-storm buildings that intersected with the extracted post-storm building footprints. Building footprints from the post-storm dataset that did not intersect with pre-storm footprints were excluded from the analysis.

### 2.3. Data Analysis

After the aerial imagery for pre- and post-Hurricane Ian was compiled, a supervised classification method via the maximum likelihood algorithm was run through ESRI's ArcGIS software. The maximum likelihood classification tool was used to perform a supervised classification of a multiband raster. The goal of the classification was to assign each cell in the study area a land cover category. Following Davis et al. [7], six classes were identified for the supervised classification of the post-Hurricane Ian imagery. The six classification categories included sand, road, water, roof, debris, and vegetation. The maximum likelihood classifier calculates the probability of the cell belonging to each class given its attribute value. Based on the Bayesian decision rule, the maximum likelihood estimates were weighted differently for each classification [35]. Each class was trained using the Image Classification Toolbar Training Sample Manager in ArcGIS and implemented to produce a rapid assessment of beach morphological changes, including debris, sand spills over roads, water, and fallen trees.

A set of 30 training samples was originally selected by drawing a polygon over a representative area of a specified class that appeared on the image. The first set of training samples was processed to identify how the algorithm handled the post-hurricane classification of the six classes of interest. Additional signature samples were collected using the methodology from Davis et al. [7]. In total, 25 samples were collected for the water category, 50 for the vegetation category, and 100 for roof, sand, debris, and road classification. The training sample classifications were converted into a signature file for use in the maximum likelihood classification, where the a priori weight was set to equal. The majority tool was used to obtain a more continuous feature boundary. Finally, the nibble tool was employed for the final post-classification generalization in which a mask was overlaid on the input raster data, specifying small pixel clusters that were replaced by the value of the closest pixel.

Although the supervised classification provides information about the extent of the overall post-landfall impact, it does not provide sufficient detail to quantify damage to structures. To examine the extent of structural damage after Hurricane Ian, LiDAR Analyst™ tools were used to extract building footprints and building heights pre- and post-storm. For quality assurance and quality control, buildings that were not identified pre-storm but extracted post-storm were removed from the analysis. The extracted building footprints were overlaid on the post-imagery to estimate the total number of damaged buildings as well as the level of damage to each structure. A classification scheme was developed based on the FEMA Preliminary Damage Assessment [36] and Davis et al. [7] to describe the damage state of the buildings. The damage probability matrix (Table 1) consisted of four damage categories: (1) 'affected' (i.e., minor observable damages); (2) 'major damage' (i.e., major roof damage but the property still habitable); (3) 'severe dam-

age’ (i.e., partial roof collapse, property not habitable); and (4) ‘destroyed’. Each damage state is associated with an example shown in Table 1. The detailed examples were used as criteria for the visual assessment of each structure and the determination of a damage score between 0 and 4. Tax appraiser data updated in 2022 from the Lee County GIS portal were used to estimate the value of the damaged properties.

**Table 1.** Building classification matrix.

| Value | Damage State | Example   |
|-------|--------------|---|
| 0     | Not Affected | Roof intact, no damage to landscape or attached structures  |
| 1     | Affected     | Roof intact with slight damage (0–30%), damage to landscape, property habitable                                   |
| 2     | Major        | Major repairs to roof over essential living space (30–50%), property habitable                                    |
| 3     | Severe       | Failure or partial failure of roof or structure, major damage to infrastructure (50–100%), property not habitable |
| 4     | Destroyed    | Destruction (100%), only foundation remains, foundation completely shifted, property not habitable                |

To further identify damages in the aftermath of Hurricane Ian, a hotspot analysis using the Getis-Ord  $G_i^*$  test statistic was conducted. The aim of the hotspot analysis was to identify the areas with the highest concentration of heavily damaged or destroyed buildings. The general G statistic was computed first to identify a fixed distance band that presented statistically significant clustering ( $p$ -value < 0.05). Then, the local Getis-Ord  $G_i^*$  statistic was used to identify structures that belonged to clusters of high and low values based on z-scores. Morphological changes to the subaerial beach were examined and compared to the damage assessment in an effort to understand the relationship between the extent of damage and beach morphological changes. BareEarth DEMs were generated to identify elevation changes in the study area by using the raster calculator tool in ArcGIS. Specifically, an algebraic expression was run to subtract the pre- and post-storm DEMs. Analysis of beach morphology was conducted by creating profile graphs to visualize elevation changes over a continuous distance. Using the Elevation Profile tool in ArcGIS, areas that represented the most severe and the least amount of damage were selected and compared to the beach profiles pre- and post-Hurricane Ian. The results from the hotspot analysis were compared to pre- and post-storm beach morphology and barrier island elevation to identify patterns of clustering of heavily and less damaged buildings.

### 3. Results

#### 3.1. Rapid Assessment through Image Classification

The image classification raster (Figure 2) shows debris, sand deposition, and flood-water patterns across Estero Island’s urbanized areas. The results indicated a significant overwash with heavy deposition of sand onto the most seaward roadway adjacent to the dunes and seawalls. The post-storm assessment also revealed heavy sand deposits on the roadways throughout the island. Ponding water was found hundreds of meters inland near buildings and other structures, providing evidence of the extent of inundation resulting from the storm. The algorithm also identified a substantial amount of debris throughout the study area, with increased amounts found inland and clustered near structures. Small amounts of debris were also present throughout the heavily vegetated areas and landward of the barrier island. The final processed raster image indicated areas that were classified as roofs in the pre-hurricane image and reclassified as debris in the post-storm image, illus-

trating the extent of the catastrophic damage to the area. The results showed substantial amounts of sediment and debris deposited across the barrier island.



**Figure 2.** Maximum likelihood algorithm results.

### 3.2. Housing Damage Assessment

The assessment of the damages to structures in the study area after Hurricane Ian was completed using aerial imagery interpretation based on the damage classification matrix shown in Table 1. A total of 2427 structures were identified after post-processing of the LiDAR point cloud data and extraction of building footprints pre- and post-Hurricane Ian (Figure 3). The analysis identified only one structure in the study area that was classified as ‘not affected’; this structure was described as a store in the land use description of the tax appraiser data (Table 2). For this structure, no visible damage was present to the property or the roof. A total of 1523 buildings were classified as ‘affected’ with a moderate level of structural damage. Overall, 734 buildings had 30–50% structural damage. They were included in the ‘major’ damage category. The majority of the structures in both the ‘affected’ and ‘major’ damage categories were single-family and multi-family (<10 units) residences. The study identified 158 buildings that were severely damaged. Most of the structures in this category had partial or complete roof failure. A total of 11 structures were classified as ‘destroyed’. Single-family and multi-family (<10 units) residences were the majority of the structures in the ‘severe damage’ and ‘destroyed’ categories.



**Figure 3.** Results of building extraction post-Hurricane Ian after QAQC of extracted buildings pre-Hurricane Ian for a total of 2427 structures identified.

Among the ‘severely damaged’ and ‘destroyed’ structures were mobile home subdivisions. There were at least seven mobile home subdivisions that were heavily impacted by the storm. It is important to note that the subdivisions do not take into consideration the individual mobile/manufactured homes present, just the land that the homes occupy. The majority of the structures that experienced 0–30% damage were classified as low-rise condominiums (<3 floors), commercial shopping centers, and stores. The 2022 tax appraiser data from the Lee County GIS portal indicated that the total market value of the damaged structures that fell into the ‘severe damage’ or ‘destroyed’ categories totaled USD 218,107,346. The estimated value of the heavily damaged single-family homes was USD 75,530,843, while the estimated value of the damaged multi-family (<10 units) residences amounted to USD 13,786,451.

A hotspot analysis using the Getis-Ord  $G_i^*$  test statistics was conducted to identify areas of significant clustering based on damage level. The results from the hotspot analysis found a significant clustering of highly damaged structures located predominantly on the north and central seaward side of the barrier island (Figure 4). Areas with high z-scores (shown in red) indicated spatial clustering of high values in relation to high damage levels. The study results also revealed significant clustering of ‘minor’ to ‘no damage’ structures predominantly on the central seaward side and landward side of the barrier island. Areas with low z-scores indicated a spatial clustering of low values (denoted in blue). Multiple areas resulted in no significant clustering with a z-score near zero, which indicated no apparent spatial clustering (shown in gray). The areas with no significant clustering were found dispersed throughout the barrier island, and the majority were located inland.

**Table 2.** Total number of structures in Estero Island, Florida, impacted by Hurricane Ian by land use description, level of damage, and assessed cumulative value.

| Use Description  | Total Number of Structures | Not Affected | Affected    | Major      | Severe     | Destroyed | Cumulative Just Value of Major-Destroyed Structures |
|--|----------------------------|--------------|-------------|------------|------------|-----------|---|
| Churches   | 11                         | 0            | 2           | 6          | 3          | 0         | 31,711,838  |
| Commercial   | 5                          | 0            | 4           | 0          | 1          | 0         |   |
| Commercial—Vacant  | 3                          | 0            | 1           | 2          | 0          | 0         |   |
| Condominiums   | 79                         | 0            | 59          | 15         | 5          | 0         | 22,167,099  |
| Condominium—High Rise (>8 Floors)                        | 38                         | 0            | 24          | 13         | 1          | 0         |   |
| Condominium—Mid Rise (4–7 Floors)                        | 73                         | 0            | 44          | 24         | 5          | 0         |   |
| Condominium—Low Rise (<3 Floors)                         | 48                         | 0            | 17          | 26         | 5          | 0         |   |
| Co-Operative (Mobile Home/Manufactured Home)             | 13                         | 0            | 4           | 1          | 7          | 1         | 690,389   |
| County Owned—Offices, Library, Government Buildings      | 6                          | 0            | 3           | 3          | 0          | 0         |   |
| Financial Institutions                                   | 3                          | 0            | 1           | 1          | 1          | 0         | 2,775,650   |
| Government Owned—Park/Recreation Area                    | 2                          | 0            | 1           | 0          | 1          | 0         | 17,069,367  |
| Marinas  | 7                          | 0            | 6           | 0          | 1          | 0         | 7,912,253   |
| Medical Office Buildings                                 | 1                          | 0            | 0           | 1          | 0          | 0         |   |
| Motels   | 15                         | 0            | 4           | 9          | 1          | 1         | 31,723,058  |
| Multi-Family (>10 Units)                                 | 1                          | 0            | 0           | 1          | 0          | 0         |   |
| Multi-Family (<10 Units)                                 | 333                        | 0            | 197         | 112        | 21         | 3         | 13,786,451  |
| Municipally Owned—Offices, Library, Government Buildings | 2                          | 0            | 1           | 1          | 0          | 0         |   |
| Office Buildings—Multi-story                             | 2                          | 0            | 1           | 0          | 1          | 0         | 2,013,485   |
| Office Buildings—One-story                               | 7                          | 0            | 4           | 0          | 3          | 0         | 2,998,838   |
| Recreational Areas                                       | 4                          | 0            | 3           | 0          | 1          | 0         |   |
| Restaurants  | 8                          | 0            | 1           | 5          | 0          | 2         | 6,997,605   |
| Schools  | 1                          | 0            | 0           | 1          | 0          | 0         |   |
| Shopping Centers   | 7                          | 0            | 1           | 5          | 1          | 0         | 656,849   |
| Single Family Residential                                | 1719                       | 0            | 1125        | 495        | 95         | 4         | 75,530,843  |
| Store, Office, Residential Combination                   | 6                          | 0            | 2           | 3          | 1          | 0         | 332,176   |
| Stores (1 Floor)   | 14                         | 1            | 5           | 5          | 3          | 0         | 1,164,892   |
| Theatres   | 1                          | 0            | 1           | 0          | 0          | 0         |   |
| Utilities  | 2                          | 0            | 2           | 0          | 0          | 0         |   |
| Residential—Vacant                                       | 15                         | 0            | 9           | 5          | 1          | 0         | 576,553   |
| Industrial   | 1                          | 0            | 1           | 0          | 0          | 0         |   |
| <b>TOTAL</b>   | <b>2427</b>                | <b>1</b>     | <b>1523</b> | <b>734</b> | <b>158</b> | <b>11</b> | <b>218,107,346</b>                                  |

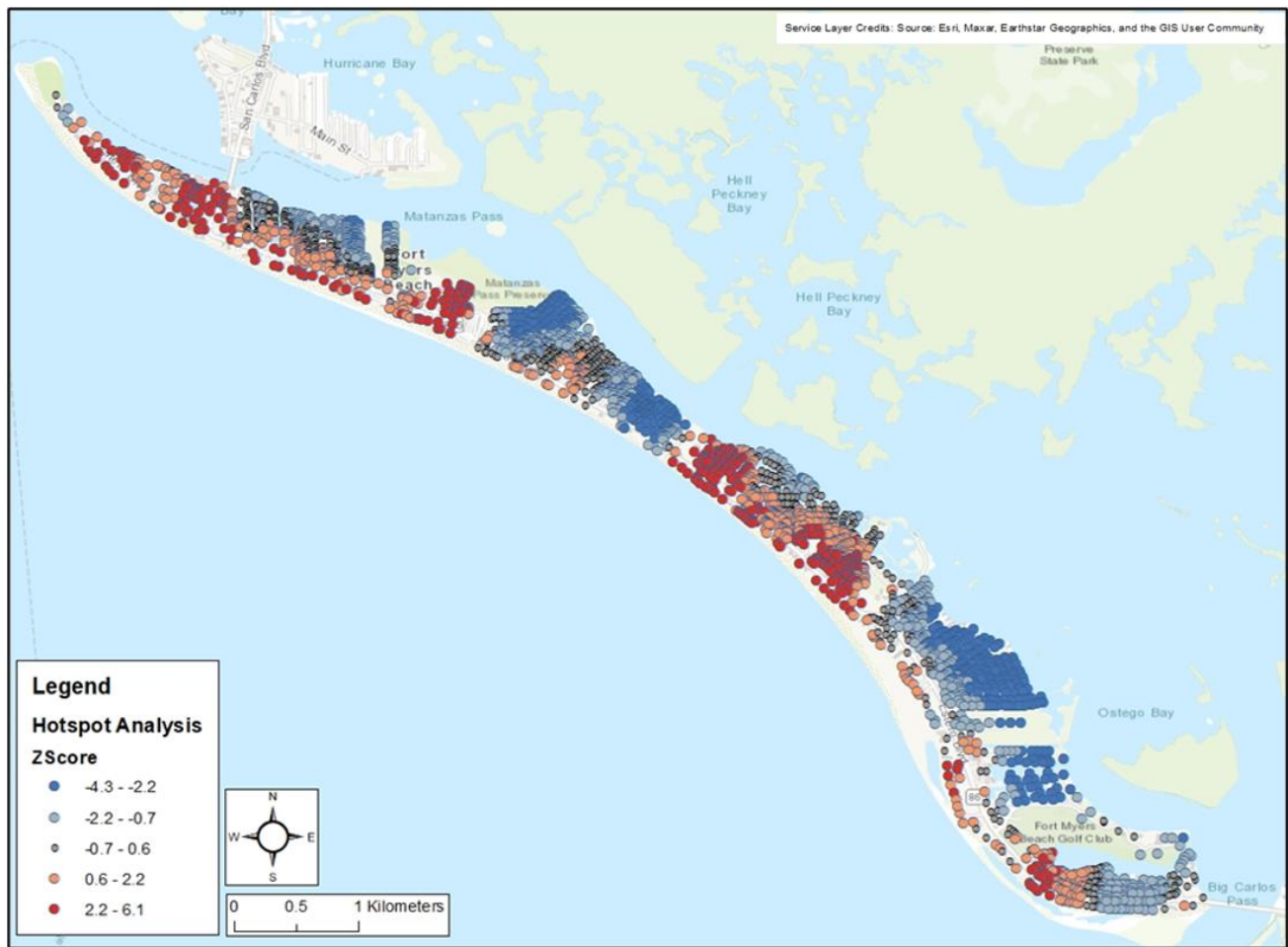


**Figure 4.** Results of hotspot analysis indicate most severe damage occurring on the seaward side of the northern and central areas of Estero Island, Florida.

### 3.3. Beach Morphology Assessment

A beach morphology analysis after Hurricane Ian showed heavy erosion to the seaward side of the island and accretion to the landward side (Figure 5). Elevation loss to the subaerial beach on the seaward side ranged from  $-1$  m to  $-5$  m. Most of the elevation gain was present on the landward side, with a gain of 2 m to 8 m. Heavy accretion was present at the northern portion of the island. A number of perpendicular washouts were found along the backbeach throughout the entire barrier island, with evidence of high erosion rates to the foreshore. The assessment identified deposition from overwash behind the backbeach/dune system adjacent to the main road. A thin ridge and runnel were present at the foreshore spanning from the northern to the central portion of the island. The southern portion of the barrier island contains multiple saltwater marshes, which experienced accretion on the seaward side of the marsh, with heavy erosion to the foreshore. Inland, the barrier island had minor elevation change with areas of heavy sediment depositions and significant erosion near structures.

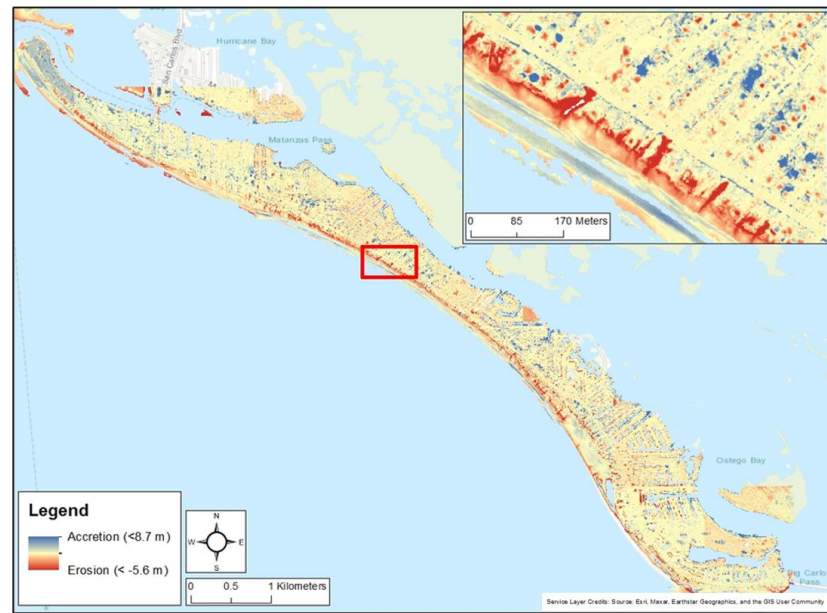


**Figure 5.** Results from DEM difference calculation indicate heavy erosion to the seaward side of the island and accretion to the landward side of Estero Island after the impacts of Hurricane Ian.

To further investigate beach response and building damage, beach profiles were extracted pre- and post-Hurricane Ian for locations with high and low damage clustering. For the purpose of this study, one area of heavily damaged structures and one area of minimally damaged structures were examined relative to beach morphology change. The areas were both located on the central portion of the island, located adjacent to one another. The northern area had considerable clustering of structures with minimum damage (Figure 6). A beach profile was extracted at the center location of both the heavily damaged area and the less damaged area to create a cross-shore transect for both pre- and post-storm beach elevations. The transect was created using pre-storm aerial imagery to identify the foredune or a topographic delineation to 0 m elevation (NAVD88). The extracted beach profiles represent changes in beach morphology pre- and post-Hurricane Ian at the selected locations.

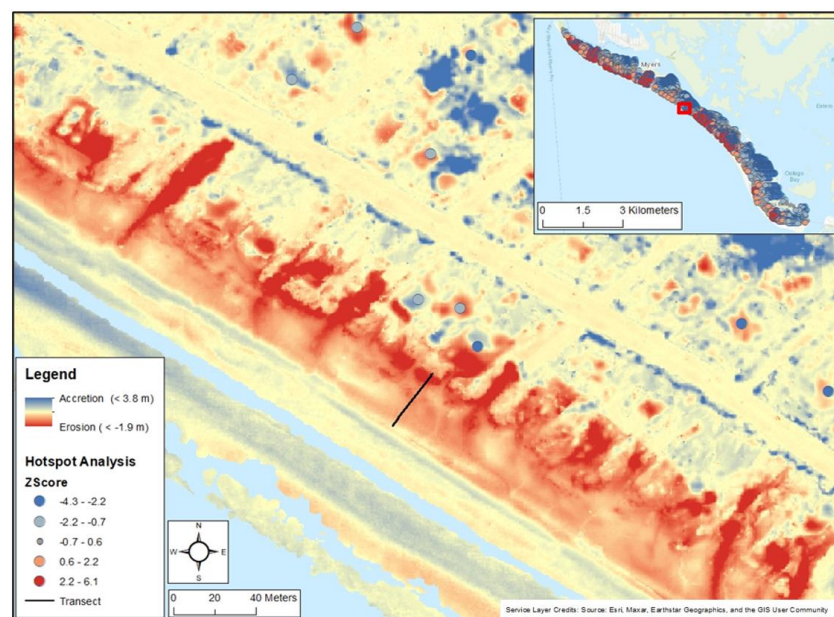


**Figure 6.** Significant clustering of an area with minimal damage to structures. Cross-shore transect represented by the black line for utilization of elevation profiles pre- and post-storm assessment.

The cross-shore transect located in the area where there was the least amount of damage represented a wide beach with a gently sloping foreshore (Figure 7). The beach profile showed a 15 m wide dune system, a 20 m berm, and a gently sloping foreshore. After Hurricane Ian, the beach maintained its width but featured a small ridge and runnel system in the intertidal zone. The berm and backbeach experienced a slight elevation loss of 0.5 m. The most notable change was a meter of elevation loss to the foredune with a 2 m wide trough seaward of the foredune.

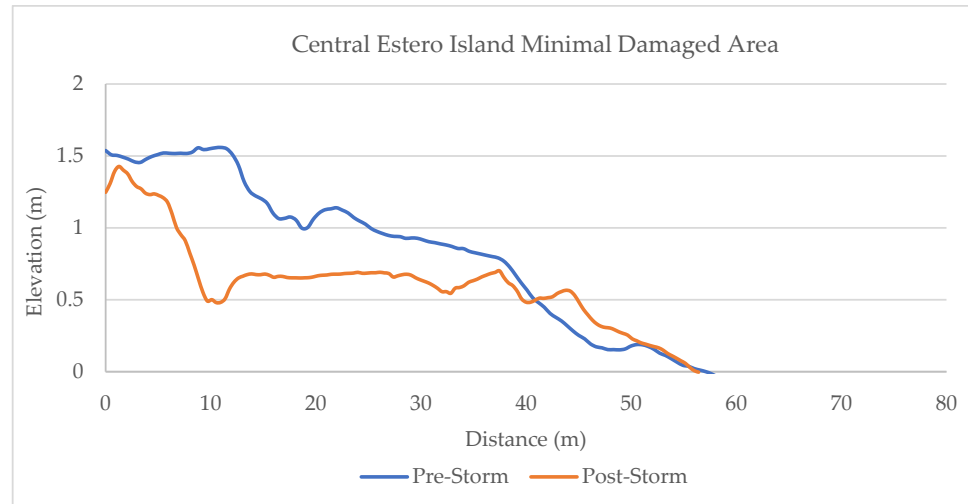


Figure 7. Beach profile for pre- and post-storm impacts for minimal damaged area.

The southern area of interest had a significant clustering of structures that had substantial damage (Figure 8). The pre-storm beach profile measured 30 m wide and had a gently sloping subaerial beach with a 0.5 m seawall located on the backbeach (Figure 9). After the hurricane, ~1 m of scouring was measured at the seawall with an ~8 m wide trough on the seawall’s seaward side, resulting in a 1 m elevation loss to the backbeach. The foreshore accreted with 30 m of seaward advance with a ridge and runnel measured in the intertidal zone.

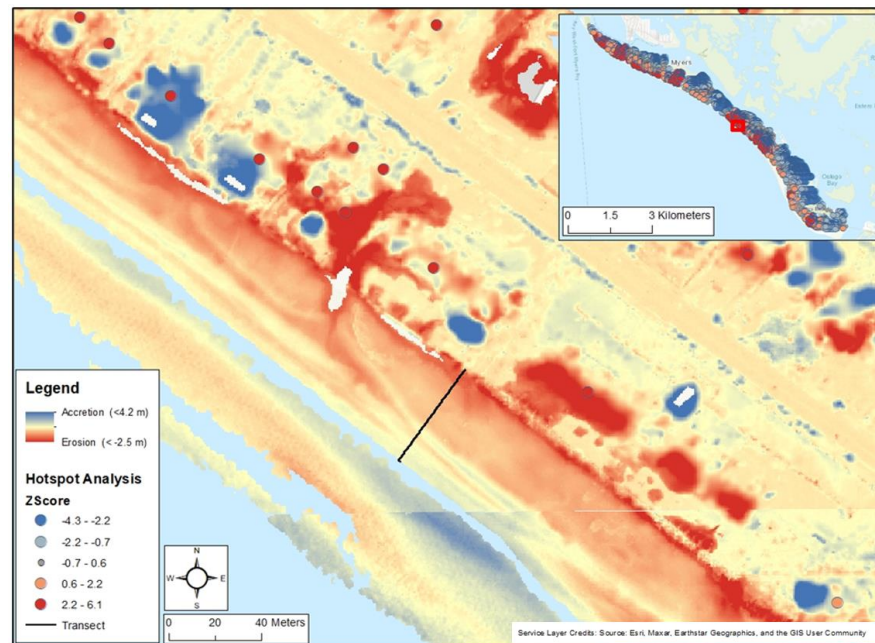
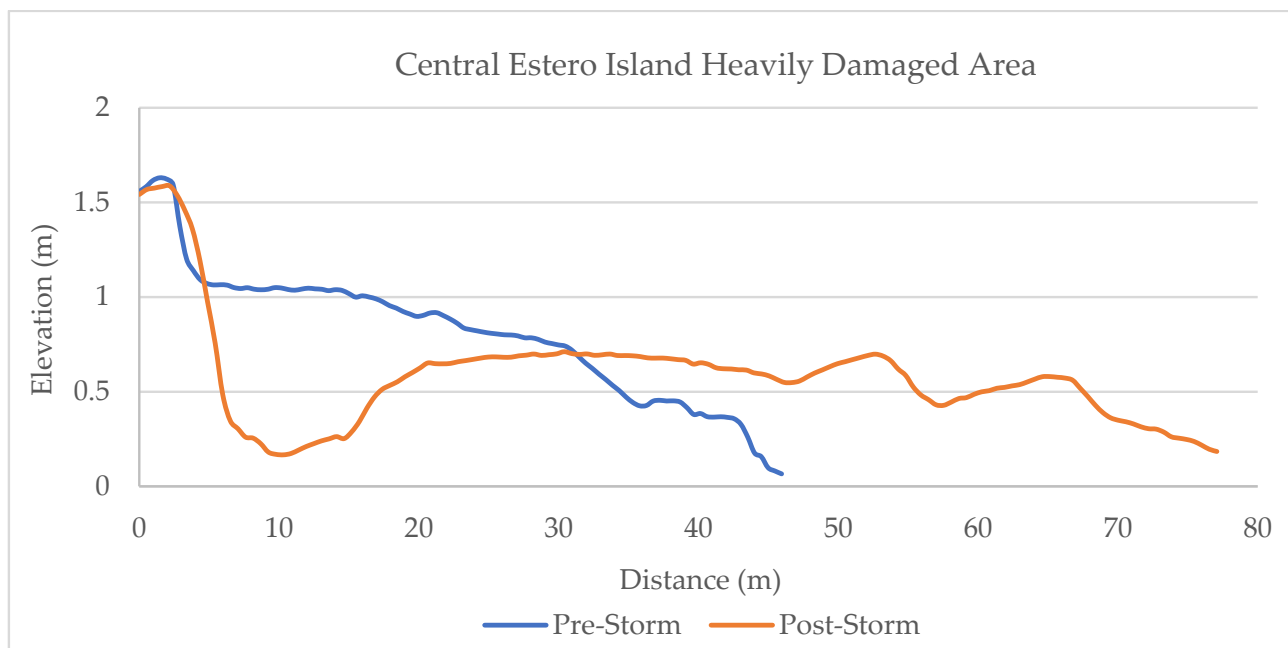


Figure 8. Significant clustering of an area with heavy damage to structures. Cross-shore transect represented by the black line for utilization of elevation profiles pre- and post-storm assessment.



**Figure 9.** Beach profile for pre- and post-storm impacts for heavily damaged area.

#### 4. Discussion

Hurricane Ian produced high wind speeds, storm surge, and flooding that caused considerable destruction throughout Estero Island, Florida. The aftermath of a severe disaster such as Hurricane Ian disrupted communication and power and created roadblocks that would result in delays in emergency post-storm assessments and response operations. Field-based emergency response assessments are critical but can be hindered by delays and other setbacks due to the severity of the damage and lack of access to the hardest hit areas. Damage assessments using NOAA's Emergency Response Imagery database in conjunction with JALBATCX airborne LiDAR data can provide valuable and pertinent information to quantify the extent of the debris fields and the magnitude of structural damages. This study identified over 2400 structures on Estero Island impacted by Hurricane Ian. Over 170 structures suffered extensive damage or were completely destroyed.

While LiDAR and aerial imagery have many advantages in identifying damaged structures and beach morphology changes, this study has several limitations. For example, the methods discussed here cannot accurately identify damages caused by storm surges and flooding. Due to the complexity associated with multiple factors resulting in structural damage, this study may have underestimated the extent of damage to a structure, which is one of the limitations of the methodologies presented here. A second limitation is the potential under- or overestimation of the property values. This study uses available data from an open GIS portal; gaps in parcel information may have influenced our estimates depending on when the parcel records were updated. The assessed market value of properties is required by law to be updated every year. Market value for a property can be determined by employing different methods and, depending on the time of assessment, can lead to fluctuations in the assessed value [37]. The appraised (just) value of a property can increase or decrease depending on a multitude of factors. For example, increases in market value changes (i.e., addition of a pool or square footage) can increase the assessed value but, after impacts from a major storm where damages are present to the structure, a decrease in just value may occur. The surrounding community economy may also influence the property value at the time of assessment [37]. This study did not take into consideration when a property was assessed for just value, which may influence the results. Future studies should be cognizant of the time properties were assessed and any major events that could contribute to value fluctuation. The results produced an estimate of the damages

and identified hotspots of severe damage across the island after Hurricane Ian based on a “bird’s eye” view. While these results can help efforts in identifying priority areas for immediate action after a disaster, full damage assessment requires field reconnaissance surveys to uncover obstacles related to ground conditions and how they would affect response and recovery operations.

The maximum likelihood algorithm performed efficiently using a series of training samples. Overall, comparing the post-aerial imagery to the algorithm model presented a slight trend toward overprocessing due to the extent of debris spread throughout the study area. The debris fields were associated with a wide range of coloration and sizes, which could have been the reason for the overprocessing errors in the classification of sand and debris. The sediment on Estero Island is very light in coloration and looks similar to some of the other classification categories, such as roadways. The algorithm also mistakenly identified vegetation and water in certain areas across the barrier island. Ponding shallow water mixed with debris takes on the coloration of a dark brown/green color, which is very similar to the training sample for the classification of vegetation. One of the most notable issues was near the foreshore, where a ridge and runnel were present. The runnel had similar coloration as the vegetation, so the training sample failed to distinguish the differences in some areas. Further analysis will help modify the training sample to identify the weights of each classification that can reduce overprocessing errors. Future assessments should include ground truthing data to improve the accuracy and validate the classification output.

The results of this study indicated that the storm impacted single-family homes and multi-family residences the most. Based on the ASCE 7 Florida Building Code, Estero Island lies within the Risk Category I–IV, and building codes require building design for wind speeds of 140–180 mph [38]. Category I includes buildings or other structures where failure is not a risk to human life, mainly for garages. Category II includes single-family homes, apartment buildings, offices, retail, and commercial buildings, while Category III refers to large occupancy structures. Finally, Category IV buildings are essential facilities like hospitals and hurricane shelters [39]. Most of the structures on Estero Island are categorized as Risk Category II, which means that buildings are required to be built to withstand wind speeds of 160 mph. However, the wind gusts of Hurricane Ian exceeded these limits. Further analysis is warranted to compare each risk category to the level of damage to understand how the current building code requirements might have impacted the level of damage after a Category 4 hurricane.

Estero Island experienced heavy erosion to the foreshore with multiple perpendicular washouts at the backbeach. The overwash regime on the barrier island was examined based on a conceptual model that scales storm impacts [40]. An overwash regime occurs when the storm surge plus wave runup overtops the foredune ridge or foredune ridges are eroded by a prolonged storm wave attack [41]. Evidence indicated that runup overtopped the dunes/topographic delineation, and water flowed landward, resulting in considerable inland sediment deposition. The nearshore environment gained elevation, indicating sediment deposition from erosion of the subaerial beach. There is a notable deposition of sediment across the roadways and on the backside of the barrier. This type of sediment deposition is not readily returned seaward to the beach under post-storm conditions, calling for substantial mitigation efforts to return lost sediment back to the beach. A ridge and runnel system across the barrier island is a common morphologic feature associated with natural post-storm sediment loss due to onshore sediment transport [41].

The results of the pre- and post-storm beach profiles of a heavily damaged area on the central part of the island indicated significant scouring near a seawall with shoreline advance and the presence of a ridge and runnel due to significant sediment loss from the scouring. The beach profile for the minimally damaged area on the central part of the island showed increased erosion to the foredune and elevation loss to the backbeach, with the beach maintaining its shoreline position with a post-storm ridge and runnel system present. The hotspot analysis showed clustering of high and low levels of damage throughout the island. The northern portion of the island was associated with significant

spatial clustering of severely damaged structures (this area is located south of an inlet). Wave-induced setup along the shoreline to the sides of the inlet channel can produce areas of increased high water level compared with the water levels in the channel [42], resulting in increased wave energy and storm surge driven onto the island from the storm. The beach morphology assessment indicated heavy accretion to the island’s northern area, where increased sediment transport inland was likely due to the processes associated with the inlet. The island’s southern portion indicated spatial clustering of slight to ‘no damage’ to structures. The southern portion of the island incorporates multiple saltwater marshes located on the seaward side of the island on the subaerial beach. With the presence of saltwater marshes, storm-wave energy may have been substantially dissipated by friction by the time the waves reached the barrier interior [41], potentially lessening the impact on the structures in that area.

Continued efforts to incorporate more cross-shore beach profiles are necessary to gain a full understanding of beach morphological response and its relationship with structural damages. The results from this study present trends across the island of low and high levels of structural damage clustering. This trend requires further investigation, particularly in the central part of the island, where an area of minimally damaged structures is adjacent to heavily damaged structures. Ground elevations from the pre-storm DEM in the central portion of the island damages were examined and compared with structural damage and the year the structures were built (Figure 10). Before Hurricane Ian, the highest ground elevation of Estero Island was <5.5 m. When overlaying the hotspot results with DEM, no evidence was found to relate the level of structural damage to ground elevation. The year built for >2400 structures ranged from <1963 to 2019. The buildings in the areas where less damage was observed were built between 1963 and 1981. Similarly, in the areas of heavy damage, the majority of the buildings were built between 1963 and 1981. The spatial distribution of ground elevation and year built indicated no apparent trends associated with these two variables.

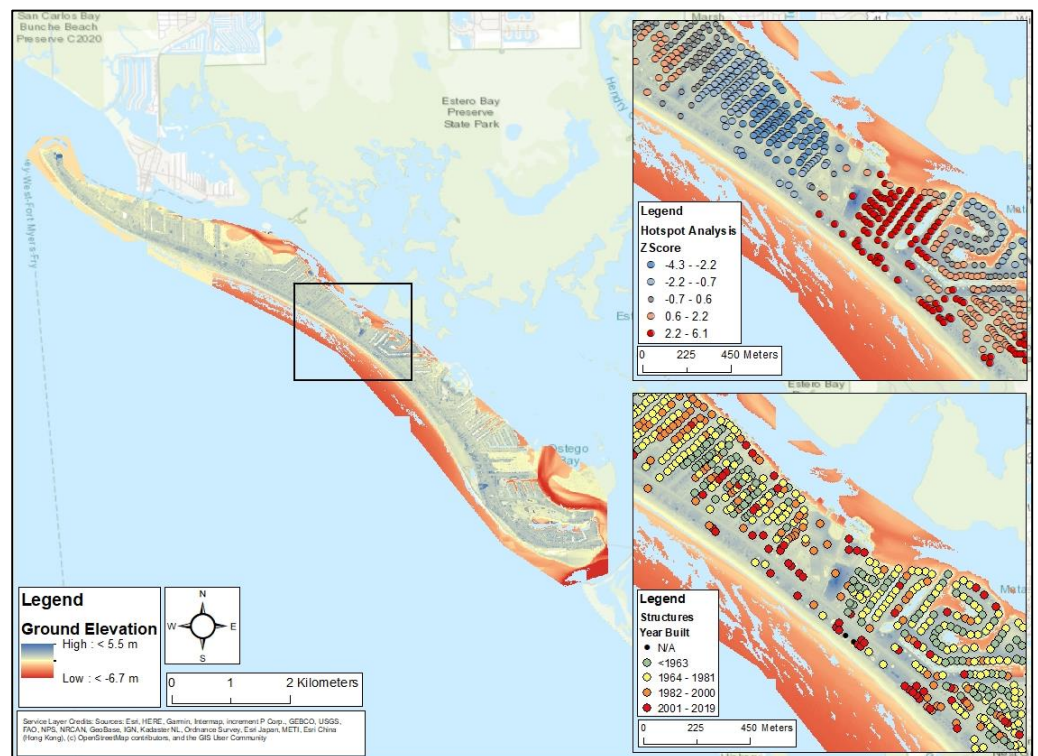


**Figure 10.** Ground elevation pre-Hurricane Ian for Estero Island compared to hotspot analysis and year built for structures for central Estero Island.

The central portion of the island is located adjacent to a backbarrier channelization connecting Matanzas Pass with Hell Peckney Bay. We have found evidence of significant clustering of heavily damaged structures south of that channelization, causing apparent channelized ebb flow that resulted in a swath of heavily damaged buildings. Ebbing surge can substantially modify morphology if the resulting current velocities are high [43]. With up to 4 m of storm surge associated with Hurricane Ian, the ebb surge may have had severe wave-induced liquefaction from the rapid decrease in water levels and influence from the adjacent channel [44]. Further research is needed to examine the role of ebbing surge (occurring after the initial storm surge) on structural damages. Future work will incorporate water level models to determine the impact of the ebb surge on damages across Estero Island.

## 5. Conclusions

This study employed JABALTCX LiDAR point cloud data and NOAA's Geodetic Survey Emergency Response Imagery database, in conjunction with Lee County tax appraiser data, to assess storm damage on Estero Island, Florida, after Category 4 Hurricane Ian. More than 2400 structures were classified, and more than 150 structures were identified as having severe damage associated with the storm. The highest percentage of damaged structures occurred on the central and northern portions of the island, where the majority of the structures were classified as single-family and multi-family (<10 units) residences. Larger structures, such as condominiums and shopping centers, were found to have less structural damage. Future analysis is warranted to examine the role of the existing building codes.

The results from the hotspot analysis indicated clusters of heavily damaged structures in the northern and central portion of the island, with damages most concentrated on the seaward side of the barrier island. Areas associated with little to no damage were spatially clustered in the southern and central portion of the island, with most structures concentrated on the landward side of the barrier island. The southern portion of Estero Island contains multiple saltwater marshes, which could have aided in the reduction in storm wave energy. A morphology assessment presented significant overwash across the island with multiple perpendicular washouts located on the backbeach. Evaluation of a cross-shore beach profile for a heavily damaged area indicated scouring to the backbeach due to the presence of a seawall with shoreline advance with a ridge and runnel after the hurricane. A cross-shore beach profile for a minimally damaged area indicated significant erosion to the foredune with elevation loss to the backbeach and the presence of a ridge and runnel. The total assessed value of the structures that were classified as heavily damaged was estimated at USD 218,107,346. The total assessed value of structures may have been underestimated due to gaps and limitations in the tax appraiser data.

The results of this study did not find evidence of associations between structural damage, on the one hand, and barrier island elevation and year built, on the other. More research is needed to examine the entire barrier island system's morphological change, as ebb surge may have been an important factor in structural damage after Hurricane Ian. The role of geomorphic influence and environmental features should be further examined to understand the role of the ebb surge in relation to structural damage. Several limitations exist within the analysis that may have produced under- or overestimation of the results. The algorithm is heavily dependent on the weights of the training sample, which can lead to interpretation errors if the weights are not adjusted accordingly. Future analysis can be improved by sensitivity analysis based on multiple training samples to identify the best outcome for the model as well as ground-truthing data to validate the model's accuracy. Future analysis will focus on multiple shore-normal transects to evaluate and compare beach morphology pre- and post-storm as it relates to the extent of damage.

Future research is needed to examine relationships between building codes, building materials, geomorphic and environmental influence, and ebb surge to improve the accuracy of post-disaster damage assessments. The damages associated with hurricanes can also influence a broad range of social, economic, and environmental variables, which are beyond the scope of this study but can be the subject of future analyses. The main contribution

of this study is to develop a conceptual framework that integrates beach morphological change, debris and sediment deposition assessment, and structural damage evaluation. The use of remote sensing data, such as aerial imagery and LiDAR, showed the potential of these technologies to advance rapid post-storm assessment and reduce the dependence on field survey methods for the collection of time-sensitive data. Despite its limitations, the study provides an integrated approach to conducting a detailed investigation of post-hurricane environmental impacts and structural damage assessment. Remote sensing technology continues to advance, and as it becomes more readily available to users, it facilitates access to a broad range of high-resolution coverage that can help prioritize emergency response efforts immediately after a catastrophic natural disaster.

**Author Contributions:** Conceptualization, L.H., D.M. and T.R.B.; methodology, L.H., D.M. and T.R.B.; software, D.M.; validation, L.H., D.M. and T.R.B.; formal analysis, L.H., D.M. and T.R.B. writing—original draft preparation, L.H.; writing—review and editing, L.H., D.M. and T.R.B.; supervision, D.M. and T.R.B.; project administration, D.M. and T.R.B. All authors have read and agreed to the published version of the manuscript.

**Funding:** This research received no external funding.

**Institutional Review Board Statement:** Not applicable.

**Informed Consent Statement:** Not applicable.

**Data Availability Statement:** The data that support the findings of this study are available from the corresponding author, [DM], upon reasonable request.

**Conflicts of Interest:** The authors declare no conflicts of interest.

## References

- NOAA. Monthly National Climate Report for September. Available online: <https://www.ncei.noaa.gov/access/monitoring/monthly-report/national/202209#:~:text=The%20contiguous%20U.S.%20average%20maximum,parts%20of%20the%20East%20Coast> (accessed on 15 December 2023).
- USGS. Hurricane Ian's Scientific Silver Lining. Coastal and Marine Hazards and Resources Program. 2023. Available online: <https://www.usgs.gov/programs/cmhrp/news/hurricane-ians-scientific-silver-lining#:~:text=%E2%80%9CWhile%20Hurricane%20Ian%20was%20undoubtedly,better%20prepared%20for%20future%20disasters.%E2%80%9D> (accessed on 15 September 2023).
- Lee County. Ian Progress Report. Available online: <https://ianprogress.leegov.com/> (accessed on 15 September 2023).
- Ball, M.M.; Shinn, E.A.; Stockman, K.W. The geological effect of hurricane Danna in Southern Florida. *J. Geol.* **1967**, *75*, 583–597. [[CrossRef](#)]
- Zhou, Z.; Gong, J.; Guo, M. Image-Based 3D Reconstruction for Post-hurricane Residential Building Damage Assessment. *J. Comput. Civ. Eng.* **2016**, *30*, 04015015. [[CrossRef](#)]
- Martin, T.; Muller, J. The geologic record of Hurricane Irma in a Southwest Florida back-barrier lagoon. *Mar. Geol.* **2021**, *441*, 106635. [[CrossRef](#)]
- Davis, J.; Mitsova, D.; Briggs, T.C.; Briggs, T.R. Post-hurricane Michael damage assessment using ADCIRC storm surge hindcast, image classification, and LiDAR. *Shore Beach* **2019**, *87*, 3–14. [[CrossRef](#)] [[PubMed](#)]
- Wang, W.; Qu, J.J.; Hao, X.; Liu, Y.; Stanturf, J.A. Post-hurricane forest damage assessment using satellite remote sensing. *Agric. For. Meteorol.* **2010**, *150*, 122–132. [[CrossRef](#)]
- Karaer, A.; Chen, M.; Gazzea, M.; Ghorbanzadeh, M.; Abichou, T.; Arghandeh, R.; Ozguven, E.E. Remote sensing-based comparative damage assessment of historical storms and hurricanes in Northwestern Florida. *Int. J. Disaster Risk Reduct.* **2022**, *72*, 102857. [[CrossRef](#)]
- Elberink, S.O.; Shoko, M.; Fathi, S.A.; Rutzinger, M. Detection of collapsed buildings by classifying segmented airborne laser scanner data. *Int. Arch. Photogramm. Remote Sens. Spat. Inf. Sci.* **2011**, *38*, 307–312. [[CrossRef](#)]
- Berezina, P.; Liu, D. Hurricane damage assessment using coupled convolutional neural networks: A case study of hurricane Michael. *Geomat. Nat. Hazards Risk* **2022**, *13*, 414–431. [[CrossRef](#)]
- Bhatt, D.; Savarese, M.; Hewitt, N.S.; Gross, A.M.; Wilder, J. Revealing the geomorphological impacts of Hurricane Ian in Southwest Florida using Geospatial Technology. *Int. Arch. Photogramm. Remote Sens. Spat. Inf. Sci.* **2023**, *48*, 43–48. [[CrossRef](#)]
- Roberston, W.V.; Zhang, K.; Whitman, D. Hurricane-induced beach change derived from airborne laser measurements near Panama City, Florida. *Mar. Geol.* **2007**, *237*, 191–205.
- Gong, J.; Maher, A. Use of mobile lidar data to assess hurricane damage and visualize community vulnerability. *J. Transp. Res. Board* **2014**, *2459*, 119–126. [[CrossRef](#)]
- Zhou, Z.; Gong, J.; Hu, X. Community-scale multi-level post-hurricane damage assessment of residential buildings using multi-temporal airborne LiDAR data. *Autom. Constr.* **2019**, *98*, 30–45. [[CrossRef](#)]

16. Battersby, S.E.; Hodgson, M.E.; Wang, J.Y. Spatial resolution imagery requirements for identifying structure damage in a hurricane disaster: A cognitive approach. *Photogramm. Eng. Remote Sens.* **2012**, *78*, 625–635. [CrossRef]
17. Xian, S.; Feng, K.; Lin, N.; Marsooli, R.; Chavas, D.; Chen, J.; Hatzikyriakou, A. Brief communication: Rapid assessment of damaged residential buildings in the Florida Keys after Hurricane Irma. *Nat. Hazards Earth Syst. Sci.* **2018**, *18*, 2041–2045. [CrossRef]
18. Luetlich, R.; Westerink, J. *Formulation and Numerical Implementation of the 2D/3D ADCIRC Finite Element Model Version 44.XX*; ADCIRC: Chapel Hill, NC, USA, 2004; pp. 1–74.
19. Mousavi, M.E.; Irish, J.L.; Frey, A.E.; Olivera, F.; Edge, B.L. Global warming and hurricanes: The potential impact of hurricane intensification and sea level rise on coastal flooding. *Clim. Chang.* **2011**, *104*, 575–597. [CrossRef]
20. Hetteren, V. Barrier Systems. In *Coastal Environments & Global Change*; Masselink, G., Gehrels, R., Eds.; Wiley & American Geophysical Union: New York, NY, USA, 2014; pp. 194–226.
21. Woodruff, J.D.; Irish, J.L.; Camargo, S.J. Coastal flooding by tropical cyclones and sea-level rise. *Nature* **2013**, *504*, 44–52. [CrossRef] [PubMed]
22. Nagarajan, S.; Khamaru, S.; De Witt, P. UAS based 3D shoreline change detection of Jupiter Inlet Lighthouse ONA after Hurricane Irma. *Int. J. Remote Sens.* **2019**, *40*, 9140–9158. [CrossRef]
23. Dean, R.G.; Malakar, S.B. Projected Flood Hazard Zones in Florida. *J. Coast. Res.* **1999**, *28*, 85–94.
24. Wohlpart, S.L.; Savarese, M.; Surge, D. The Development of Estuarine Systems in Southwest Florida: A Perspective from the Late Holocene History of Oyster Reef Development. In Proceedings of the Geological Society of America Annual Meeting Exposition, Denver, CO, USA, 29 October 2007.
25. Sambrook Smith, G.H.; Best, J.L.; Ashworth, P.J.; Fielding, C.R.; Goodbred, S.L.; Prokocki, E.W. Fluvial form in modern continental sedimentary basins: Distributive fluvial systems: Comment. *Geology* **2010**, *38*, 230–231. [CrossRef]
26. Brutsché, K.E. First Year Sedimentological Characteristics and Morphological Evolution of an Artificial Berm at Fort Myers Beach, Florida. Master's Thesis, University of South Florida, Tampa, FL, USA, 2011.
27. NOAA, National Data Buoy Center. Available online: [https://www.ndbc.noaa.gov/station\\_page.php?station=bgcfl](https://www.ndbc.noaa.gov/station_page.php?station=bgcfl) (accessed on 23 August 2023).
28. Coastal Engineering Consultants Inc. *Estero Island Restoration, 2020 Annual Monitoring Report*; Lee County Board of County Commissioners: Fort Myers, FL, USA, 2020; CEC File No. 20.079.
29. Houston, J. The value of beach nourishment on a complex shoreline. *Shore Beach* **2022**, *90*, 3–15. [CrossRef]
30. U.S. Census Bureau: American Community Survey 5-Year Estimates. Available online: <https://www.census.gov/data/developers/data-sets/acs-5year.html> (accessed on 10 December 2023).
31. Bucci, L.; Alaka, L.; Hagen, A.; Delgado, S.; Beven, J. *National Hurricane Center Tropical Cyclone Report. Hurricane Ian (AL092022)*; National Hurricane Center: Miami, FL, USA, 2022; pp. 1–72.
32. Lee County Parks & Beaches: Ian Progress Report. Available online: <https://ianprogress.leegov.com/pages/parks-beaches> (accessed on 23 August 2023).
33. National Geodetic Survey, 2022: NOAA NGS Emergency Response Imagery: Hurricane Ian, 23 September 2022 to 30 September 2022. NOAA National Centers for Environmental Information. Available online: <https://storms.ngs.noaa.gov/storms/ian/index.html#9/26.42/-81.97> (accessed on 14 December 2022).
34. Sylvester, C.; Wozencraft, J.; Robertson, Q.; Dong, Z.; Dunkin, L. JALBTCX rapid-response aerial survey reconnaissance missions. *Shore Beach* **2023**, *91*, 39–45. [CrossRef]
35. ARCGIS Pro: Performing the Classification. Available online: <https://pro.arcgis.com/en/pro-app/latest/tool-reference/spatial-analyst/performing-the-classification.htm> (accessed on 10 January 2023).
36. FEMA. *2021 Preliminary Damage Assessment Guide*; FEMA: Hyattsville, MD, USA, 2020; pp. 1–127.
37. Lee County Property Appraiser. Available online: <https://www.leepa.org/FAQ/FAQForm.aspx#MarketValue> (accessed on 12 April 2024).
38. International Code Council (ICC). 2020 Florida Building Code. In *ICC Digital Codes*, 7th ed.; International Code Council (ICC): Washington, DC, USA, 2020.
39. Ylipelkonen, R. Building Risk Categories. Available online: <https://www.floridarroof.com/building-risk-categories> (accessed on 10 December 2023).
40. Sallenger, A.H. Storm Impact Scale for Barrier Islands. *J. Coast. Res.* **2000**, *16*, 890–895.
41. Wang, P.; Roberts Briggs, T.M. Storm-Induced Morphology Changes along Barrier Islands and Post-storm Recovery. In *Coastal and Marine Hazards, Risks, and Disasters*; Ellis, J.T., Sherman, D.J., Eds.; Elsevier Inc.: Amsterdam, The Netherlands, 2015; pp. 271–306.
42. Orescanin, M.; Raubenheimer, B.; Elgar, S. Observations of wave effects on inlet circulation. *Cont. Shelf Res.* **2014**, *82*, 37–42. [CrossRef]
43. Sherman, D.J.; Hales, B.U.; Potts, M.K.; Ellis, J.T.; Liu, H.; Houser, C. Impacts of Hurricane Ike on the beaches of the Bolivar Peninsula, TX, USA. *Geomorphology* **2013**, *199*, 62–81. [CrossRef]
44. Robertson, I.N.; Riggs, H.R.; Solomon, Y.; Young, Y.L. Lessons from Hurricane Katrina Storm Surge on Bridges and Buildings. *J. Waterw. Port Coast. Ocean. Eng.* **2007**, *133*, 463–483. [CrossRef]

**Disclaimer/Publisher's Note:** The statements, opinions and data contained in all publications are solely those of the individual author(s) and contributor(s) and not of MDPI and/or the editor(s). MDPI and/or the editor(s) disclaim responsibility for any injury to people or property resulting from any ideas, methods, instructions or products referred to in the content.